HO photodissociation dynamics based on potential energy surfaces from density functional calcualtions.

Doublet, M.L.; Kroes, G.J.; Baerends, E.J.; Rosa, A.

published in
Journal of Chemical Physics
1995

DOI (link to publisher)
10.1063/1.469675

document version
Publisher's PDF, also known as Version of record

H_2O photodissociation dynamics based on potential energy surfaces from density functional calculations

M. L. Doublet, G. J. Kroes, and E. J. Baerends
Theoretische Chemie, Vrije Universiteit, De Boelelaan 1083, 1081 HV Amsterdam, The Netherlands

A. Rosa
Dipartimento di Chimica, Università della Basilicata, Via N. Sauro, 85, 85100 Potenza, Italy

(Received 3 April 1995; accepted 9 May 1995)

We investigate the usefulness of density functional theory (DFT) for calculating excited state potential energy surfaces. In the DFT calculations, the generalized gradient approximation (GGA) is used. As a test case, the photodissociation of H_2O through the first excited $\tilde{A}\ ^1B_1$ state was considered. Two-dimensional potential energy surfaces were obtained for both the $\tilde{X}\ ^1A_1$ ground state and the first excited state. Wave packet calculations employing these surfaces were used to obtain both the absorption spectrum and partial photodissociation cross sections, which are resolved with respect to the final vibrational state of the OH fragment. Comparisons are made with a previously calculated high level *ab initio* potential energy surface, with dynamics calculations using that surface, and with experiment. The vertical excitation energy for the ($\tilde{X}\ ^1A_1 \rightarrow \tilde{A}\ ^1B_1$) transition calculated using DFT is in good agreement with the previous *ab initio* calculations. The absorption spectrum and the partial cross sections obtained with the DFT treatment are in good agreement with experiment.

I. INTRODUCTION

Density functional theory (DFT) has proven itself a powerful tool for calculations of molecular ground state energies.[1,2] The Hohenberg–Kohn theorem[3] stipulates that the ground state energy of an interacting many particle system with a given fixed interparticle interaction and a local one-particle potential is uniquely determined by its (diagonal) ground state density, and that there exists a well-defined density functional for the energy that attains a minimum for the exact ground state density. The theorem does not in itself provide the tools to carry out the required energy minimization and the successes to date testify to the accuracy of approximate exchange-correlation energy functionals that have been formulated, in particular the new generation of so-called generalized gradient approximations (GGAs).[4,5] Evidence is accumulating that ground state potential energy curves can be described quite accurately with the current GGA functionals, even when transition state barriers in a reaction path are involved.[6] We are dealing here with situations where considerable configuration mixing would occur in a wavefunction treatment, and it is gratifying that the one-determinantal Kohn–Sham treatment leads to good results. (Of course the Kohn–Sham determinant is not a good approximation at all to the wave function in these cases.)

While DFT performs quite well in calculations of molecular ground states, the situation is much less clear-cut for excited state energies. Gross and co-workers[7] have formulated a density functional theory for excited states. However, the functionals that are defined are not known, in particular not the dependence on the ensemble weights that play a role in the theory. Applying just the existing functionals leads to rather poor agreement with experiment.[8]

Until now, the method used most widely in excited state calculations on molecules has been the one introduced originally by Ziegler *et al.*[9] These authors pointed out that some conditions on which the $\rho^{1/3}$ local density approximation (LDA) for the exchange potential is based are not always fulfilled, for instance in states (and in the average-of-configuration) in which the pair-correlation factor is off-diagonal in the spin. Since one-determinantal states do not present problems in this respect, they suggested to restrict the use of the LDA to one-determinantal states. Since nonlocal GGA corrections are added to the LDA, it may be preferable to apply the same restriction when using GGAs. A one-determinantal state that is used may either be a pure multiplet component or an appropriate linear combination of states belonging to different multiplets (i.e., having different symmetries). Multiplet splittings can then usually be resolved by solving a small set of linear equations. If the excited state being calculated is the lowest state of a given symmetry and symmetry permits its description by a single determinant, the method obviously is equivalent to applying a Kohn–Sham treatment to this state. In this case there is the theoretical justification that the Hohenberg–Kohn theorems can be shown to hold for the first excited state of a given symmetry.[10] A single-determinantal treatment of such states may be considered to have the same status as the Kohn–Sham treatment of ground state densities. The method of Ziegler *et al.*[9] has been shown to lead to quite good excitation energies and multiplet splittings for many molecules.[9,11] It has been applied to multiplet splittings in atoms by von Barth,[10] Lannoo, Baraff, and Schlüter[6] and Wood.[12]

An extension of the application of the method of Ziegler *et al.*[9] to the calculation of potential energy surfaces is of interest for two reasons. First, it would be extremely useful to validate the Kohn–Sham treatment for excited state potential energy surfaces, in view of the possible application to photochemistry and photophysics of large systems possessing a high degree of symmetry [e.g., organometallic system such as $Ru(bipyridine)_3^{3+}$ and $Mn_2(CO)_{10}$]. For such systems,

 0021-9606/95/103(7)/2538/10/$6.00

it may well be possible to obtain accurate potential energy surfaces for excited states relevant to the photodissociation, especially in geometries representative of bond breaking situations in which all or part of the symmetry of the system is conserved. Second, details of excited state potential energy surfaces of small systems in the gas phase are more readily amenable to experimental investigation than the ground state surfaces that play a role in reactions in solution. A study of an excited state surface, including the short distance repulsive parts, possible barriers or saddle points, and the long range dissociation region, therefore also has relevance for applications to ground state surfaces and reactivity.

As a test case, we consider the potential energy surface of the water molecule in its first excited $\tilde{A}\ ^1B_1$ state. On this surface, dissociation proceeds in a direct fashion upon excitation from the electronic ($\tilde{X}\ ^1A_1$) ground state with UV light at 165 nm. The electronic ground and first excited state are of different symmetry also under C_s (for dissociating geometries), so that a DFT treatment is justified. The photodissociation of H_2O through its first excited state is a benchmark problem for which many experiments are available;[13–18] for a recent review see Ref. 19. For the $\tilde{A}\ ^1B_1$ state, an accurate *ab initio* (CEPA-SD) potential energy surface (PES) is available from the calculations by Staemmler and Palma,[20] thus allowing a direct comparison of our DFT results for this state with high level *ab initio* calculations. In addition, the fit of Engel *et al.*[21] of the excited state PES has been used in numerous dynamical studies of the photodissociation.[17,18,21–28] With little if any exceptions, the *ab initio* calculations reproduce the experimental data on a quantitative level.[19]

As a further test of the DFT treatment, we will also show results of wave packet calculations using the excited state DFT potential energy surface, comparing both directly with experiment and with wave packet results[22] of dynamics calculations performed on the CEPA surface.[20] More precisely, we calculate both the absorption spectrum and partial cross sections for photodissociation which are resolved with respect to the vibrational state of the OH ($X\ ^2\Pi$) fragment. The calculations are performed in a two-dimensional (2D) treatment, where we freeze the bending angle at its ground state equilibrium value, also using the light–heavy–light (LHL) approximation. Previous calculations have shown these approximations to work well both for calculating the absorption spectrum[22] and for calculating vibrational partial cross sections.[29] The dynamics calculations are done within a ''full DFT treatment,'' in that the electronic ground ($\tilde{X}\ ^1A_1$) state PES (used to generate the initial vibrational state) was also taken from DFT calculations. In this sense our calculations present a more severe test of the electronic structure method used than the previous dynamics calculations, which employed an empirical surface for the ground state.

II. METHOD

A. Density functional calculations

The calculations reported in this paper are based on the Amsterdam Density Functional program package,[30] characterized by an accurate three-dimensional numerical integration procedure to obtain the Hamiltonian matrix elements[31] and a density fitting procedure to obtain accurate Coulomb potentials. The exchange-correlation functionals contain nonlocal corrections to the local-density approximation (LDA). For the latter, the parametrization of Vosko, Wilk, and Nusair[32] has been used, for the former the generalized gradient approximation for exchange by Becke[4] and for correlation by Perdew[5] have been used.

TABLE I. Exponents of the triple-ζ Slater-type orbital basis set and polarization functions used for oxygen and hydrogen atoms.

Atom	$1s$	$2s$	$2p$	$3d$	$4f$
Oxygen	core	1.72	1.12	2.00	3.00
	core	2.88	2.08		
	core	7.58	4.08		
Hydrogen	0.69	1.25	2.50		
	0.92				
	1.58				

Both the oxygen and hydrogen atoms were described by an uncontracted triple-ζ STO (Slater-type orbital) basis set augmented by one $2p$ polarization function on H, and one $3d$ and one $4f$ polarization function on O. The two $1s$ electrons of the oxygen atom have been assigned to the core and have been treated by the frozen-core approximation.[30] All the parameters describing the basis set are reported in Table I. In order to fit the molecular density, a set of auxiliary s, p, d, f, and g STO functions centered on all nuclei are used.

For the subsequent dynamics calculations, we need potential energy surfaces for both the ground $^1A_1$ state and the first excited $^1B_1$ state of water molecule. The electronic configurations of these two states are given in the C_{2v} symmetry by

$$\tilde{X}\ ^1A_1 \quad 1a_1^2 2a_1^2 1b_2^2 3a_1^2 1b_1^2, \tag{2.1a}$$

$$\tilde{A}\ ^1B_1 \quad 1a_1^2 2a_1^2 1b_2^2 3a_1^2 1b_1 4a_1. \tag{2.1b}$$

One cannot simply obtain the energy of the open-shell singlet state from the...$(1b_1\alpha)(4a_1\beta)$ determinant, since this is a mixture of singlet and triplet states. We therefore first obtain the self-consistent field (SCF) orbitals of the excited state by performing a spin-restricted SCF calculation on the excited state configuration. Next the GGA energies of single-determinantal states are calculated from the spin densities and total densities resulting from occupying these orbitals with electrons of appropriate spin. In the present case only the determinants...$(1b_1\alpha)(4a_1\beta)$ and...$(1b_1\alpha)(4a_1\alpha)$ are needed. It is of course possible to perform separate optimizations on the orbitals of these determinants, but in that case the triplet described by $(1b_1\alpha)(4a_1\alpha)$ does not strictly correspond to the triplet contained in...$(1b_1\alpha)(4a_1\beta)$, since the orbitals in the two determinants are different. For this reason no further optimizations are performed, and we use one and the same set of ''average-of-configuration'' orbitals to obtain the energy of the $1\ ^3B_1$ state and of a state which is an equal mixture of the $1\ ^3B_1$ state and the $\tilde{A}\ ^1B_1$ state. The energy of the $\tilde{A}\ ^1B_1$ state is then obtained using subtraction.

We have generated 2D potential energy surfaces for both the $^1A_1$ and $^1B_1$ states for the dynamics calculations using a grid of points in the range $[1.3a_0-4.0a_0]$ for both the O–H

bond lengths. In order to use these PESs in the dynamics calculations, we need them in an analytic form. The procedure used is described in the next section.

B. Analytic fits

The method we used to fit the calculated ground state and first excited state PESs bears a close resemblance to the method used by Engel *et al.*[21] to fit the CEPA results of Staemmler and Palma[20] for the $1\,^1B_1$ PES. The potential is written as

$$V(r_1,r_2,\alpha_e)=V_3(r_1,r_2)+V_2(r_1,r_2)+V_{\rm dis}, \tag{2.2}$$

where V_3 defines a three-body potential, V_2 defines a sum of two-body potentials, and $V_{\rm dis}$ is the electronic dissociation energy for dissociation into O+H+H [we use $V_{\rm dis}=10.08$ eV (Ref. 33)]. The two-body potentials have been constructed using Morse-potentials with the same parameters as used by Engel *et al.* ($D_{\rm OH}=4.621$ eV, $\beta_{\rm OH}=2.294$ Å^{-1}, $R_{\rm OH}=0.971$ Å) and are simply written

$$V_2(r_1,r_2)=V_{\rm Morse}(r_1;D_{\rm OH},\beta_{\rm OH},R_{\rm OH}) + V_{\rm Morse}(r_2;D_{\rm OH},\beta_{\rm OH},R_{\rm OH}). \tag{2.3}$$

Using $V_{\rm dis}=10.08$ eV and the two-body expression of Eq. (2.3) ensures that the PESs show a qualitatively correct asymptotic behavior, and the actual fitting is done using the three-body expression

$$V_3(r_1,r_2)=\sum_{i=1}^{16} c_i P_i(s_1,s_2)[1-\tanh(\alpha s_1)] \times[1-\tanh(\alpha s_2)] f_{\rm sw}(r_1) f_{\rm sw}(r_2), \tag{2.4}$$

where P_i is a polynomial up to sixth order in the variables r_1 and r_2 ($s_i=r_i-1.0$ Å as used by Engel *et al.*,[21] and we use $\alpha=1.75$ Å^{-1}). The reference point for the PESs was taken by setting $V(r_e,r_e,\alpha_e)=0$ for the A_1 ground state PES. The data points used to fit V_3 only cover the range 1.3–$4.0a_0$ for both r_1 and r_2, and to avoid artefacts in its extrapolation it is switched off smoothly for larger r values using the function

$$f_{\rm sw}(r_i)=1, \quad r_i \leqslant r_0-\Delta r \tag{2.5a}$$

$$f_{\rm sw}(r_i)=\tfrac{1}{2}+\tfrac{1}{2}\cos(\xi), \quad r_0-\Delta r<r_i\leqslant r_0+\Delta r \tag{2.5b}$$

$$f_{\rm sw}(r_i)=0, \quad r_i>r_0+\Delta r \tag{2.5c}$$

$$\xi=\frac{[r_i-(r_0-\Delta r)]\pi}{2\Delta r} \tag{2.5d}$$

using $r_0=5\ a_0$ and $\Delta r=1\ a_0$.

C. Dynamics

In a time dependent formalism, Fermi's golden rule for the total cross section for photodissociation can be written in SI units as[34,35]

$$\sigma(E)=\frac{\pi\nu}{3c\epsilon_0\hbar}\int_{t=-\infty}^{\infty}\exp(iEt/\hbar) \times\langle\Phi(r_1,r_2,t=0)|\Phi(r_1,r_2,t)\rangle dt \tag{2.6}$$

with

$$\Phi(r_1,r_2,t=0)=\mu(r_1,r_2)\Psi_i(r_1,r_2). \tag{2.7}$$

In Eqs. (2.6) and (2.7), ν is the frequency of the exciting radiation, and $E=E_i+h\nu$ is the total energy, where E_i is the initial energy (electronic+vibrational) of the absorbing molecule. Furthermore, $\Psi_i(r_1,r_2)$ is the nuclear (vibrational) wave function of the absorbing molecule in its ground electronic state and $\mu(r_1,r_2)$ is the transition dipole moment function. In a wave packet calculation, the autocorrelation function $\langle\Phi(t=0)|\Phi(t)\rangle$ is obtained by propagating the initial wave packet given by Eq. (2.7) using the Hamiltonian for nuclear motion appropriate to the excited electronic state, which is given by

$$\hat{H}=-\frac{\hbar^2}{2\mu_d}\frac{\partial^2}{\partial r_1^2}-\frac{\hbar^2}{2\mu_d}\frac{\partial^2}{\partial r_2^2}+V(r_1,r_2,\alpha_e). \tag{2.8}$$

In writing Eq. (2.8), the light–heavy–light (LHL) approximation[36] has been used. Furthermore, μ_d denotes the reduced mass of the OH diatomic fragment, and α_e is the equilibrium bond angle of H_2O in its ground electronic state. Finally, $V(r_1,r_2,\alpha_e)$ is the excited state potential energy surface calculated as described in Sec. II A and fitted as described in Sec. II B.

Partial cross sections that are resolved with respect to the final vibrational state of the diatomic fragment can be obtained by analyzing the wave packet along a cut in coordinate space corresponding to a large value of the scattering coordinate.[35,37] The wave packet $\Phi(r_1,r_2,t)$ is projected on the vibrational fragment eigenstates at $r_1=R_\infty$ using

$$\Phi(R_\infty,r_2,t)=\sum_v C_v(R_\infty,t)\phi_v(r_2) \tag{2.9}$$

with

$$C_v(R_\infty,t)=\langle\phi_v(r_2)|\Phi(R_\infty,r_2,t)\rangle, \tag{2.10}$$

where $\phi_v(r_2)$ is a normalized vibrational wave function for the diatomic fragment. After obtaining the half-transform of $C_v(R_\infty,t)$ as

$$A_v(R_\infty,E)=\frac{1}{2\pi}\int_{t=0}^{\infty}\exp(iEt/\hbar)C_v(R_\infty,t)dt \tag{2.11}$$

partial cross sections for photodissociation are calculated in SI units as[37]

$$\sigma_v(E)=2\,\frac{4\pi^3\nu k_v}{3c\epsilon_0\mu_d}\,|A_v(R_\infty,E)|^2, \tag{2.12}$$

where k_v is given by

$$k_v=\frac{\sqrt{2\mu_d(E-\epsilon_v)}}{\hbar}. \tag{2.13}$$

In Eq. (2.13), ϵ_v is the total (electronic+vibrational) energy of the diatomic fragment in its (v) state. In Eq. (2.12) the added factor 2 takes into account that dissociation of H_2O can result in either one of two different, but undistinguishable OH fragments.

The calculation of the photodissociation cross sections requires the ground state vibrational wave function

TABLE II. Numerical values of the parameters used in the variational and wave packet calculations are given. The parameters f_{rr}, D_e, and $R_e(r_e)$ describe the Morse oscillator functions used in the variational calculation (see Ref. 39). For the meaning of the other parameters, see the text. The time step is in atomic units, where 1 atomic unit of time $\approx 2.419\times10^{-2}$ fs.

Parameter	Value
N_m	7
M_1	20
f_{rr}(aJ/Å^2)	8.454
D_e(cm^{-1})	37 354
r_e(Å)	0.96
N_R	128
$R_{\min}(a_0)$	1.0
$R_{\max}(a_0)$	10.0
N_L	9
N_s	2 500
Δt	2.00
$x_1(a_0)$	8.0
$x_2(a_0)$	10.0
$R_\infty(a_0)$	7.96

TABLE III. Experimental and theoretical values of the vertical excitation energy T_v associated with the ($\tilde{X}\ ^1A_1 \rightarrow \tilde{A}\ ^1B_1$) transition in H_2O, and of the electronic energy release $E_{\rm rel}$. The bond angle is 104.52°.

Method	R_{O-H} (a_0)	T_V (eV)	$E_{\rm rel}$ (eV)	Ref.
DFT	1.836	7.58	2.04	
CEPA	1.8088	7.52	2.35	20
DFT	1.8088	7.69	2.22	
Expt.		7.70[a]	2.30[a]	13

[a]These two values have been obtained by comparing the experimental and theoretical absorption spectrum, as discussed in Sec. III C.

$\Psi_i(r_1,r_2)$ associated with the electronic ground state and its energy as input [see Eqs. (2.6) and (2.7)]. To obtain this wave function, a variational calculation was performed using the Hamiltonian of Eq. (2.8), where $V(r_1,r_2,\alpha_e)$ denotes the electronic ground state potential energy surface which is calculated as described in Sec. II A and fitted as described in Sec. II B. The method used in the variational calculation is basically that of Tennyson and Sutcliffe,[38] except that as basis functions for the r_1 and r_2 coordinates we simply employ Morse oscillator functions as described in Ref. 39. In the variational calculation, we used N_m Morse oscillator functions as basis functions for the r_1 and r_2 coordinates, and the integration over the potential was performed using M point Gauss–Laguerre quadrature. For the numerical values used for these parameters and the parameters describing the Morse oscillator functions in the 3D calculations, see Table II.

In order to compute $\Phi(r_1,r_2,t)$ of Eq. (2.6), the wave function $\Psi_i(r_1,r_2)$ as obtained variationally is calculated on a grid and multiplied with the transition dipole moment function $\mu(r_1,r_2)$, thus obtaining $\Phi(r_1,r_2,t=0)$. For the transition dipole moment function $\mu(r_1,r_2)$, we use the constant value $\mu=0.483$ atomic units, which is the *ab initio* value at the electronic ground state equilibrium geometry.[21] Due to the fairly weak dependence of the transition dipole moment on the nuclear coordinates in the Franck–Condon region, using a constant transition dipole moment is a reasonable approximation.[21] The grid consists of $N_R\times N_R$ points in r_1 and r_2. We employ equal spacing in r_1 and r_2, the grid points lying in the range ($R_{\min}$,$R_{\max}$) (see Table II for the actual values used in the calculation).

To propagate the wave function in time, we used the short iterative Lanczos (SIL) integrator[40] of order N_L, taking N_s time steps of size Δt (see Table II). In performing the Hamiltonian operation on the wave function, the action of the kinetic energy operators is evaluated using the fast Fourier transform (FFT) algorithm.[41] After every two time steps, the overlap of the wave packet $\Phi(r_1,r_2,t)$ with $\Phi(r_1,r_2,0)$ and the coefficients C_v are calculated and stored (see Table II for the value used for R_∞). To keep the wave function from traversing the grid boundaries at longer times, after every two consecutive time steps the wave function is multiplied with an absorption function for values of r_1 and r_2 between x_1 and x_2 (see Table II), using the absorption function defined in Eqs. (9) and (10) of Ref. 42.

The diatomic fragment eigenstates $\phi_v(r_2)$ required for calculating v-resolved cross sections [see Eq. (2.10)] were calculated using a discrete variable representation (DVR) type method.[43,44] The same grid points in r_2 were used as in the dynamics calculations. The potential used for the diatomic fragment is the Morse-potential describing the asymptotic OH fragment in the fit of the excited state H_2O potential (see Sec. II B). The calculated eigenvalues and eigenfunctions showed excellent agreement with the analytical results for the Morse potential.

III. RESULTS AND DISCUSSION

A. DFT calculations

Theoretical values for the vertical excitation energy T_v and the electronic energy release $E_{\rm rel}$ upon dissociation in the $^1B_1$ state are given in Table III, also comparing with estimates obtained by combining results of experiments and dynamics calculations (see Sec. III C for how the estimate was obtained). For comparison we also give the results of previous CEPA calculations by Staemmler and Palma.[20] The vertical excitation energy T_v has been obtained by subtracting the ground $^1A_1$ state energy from the excited $^1B_1$ state energy in the optimized ground state geometry of H_2O, described by two equivalent 1.836 a_0 O–H bond distances, where we keep the bond angle fixed at its ground state equilibrium value of 104.52 deg.[20] The value thus obtained (7.58 eV) is slightly higher than the value previously obtained in the CEPA calculations (7.52 eV, Ref. 20). Both values for T_v are lower than the experimental value (7.7 eV). Our ground state equilibrium geometry slightly differs from the geometry for which Staemmler and Palma give their value of T_v ($r_1=r_2=1.8088\ a_0$, same bond angle), and we also give the value we calculate for the energy difference for this geometry in Table III.

The electronic energy release $E_{\rm rel}$ is provided by the difference between the electronic energies of $^1B_1$ state at the ground state equilibrium geometry and at dissociation [the electronic energy of the OH($^2\Pi$) and H(^2S) fragments]. The DFT calculated electronic energy release is smaller than the CEPA calculated one (2.04 eV vs 2.35 eV) and in worse

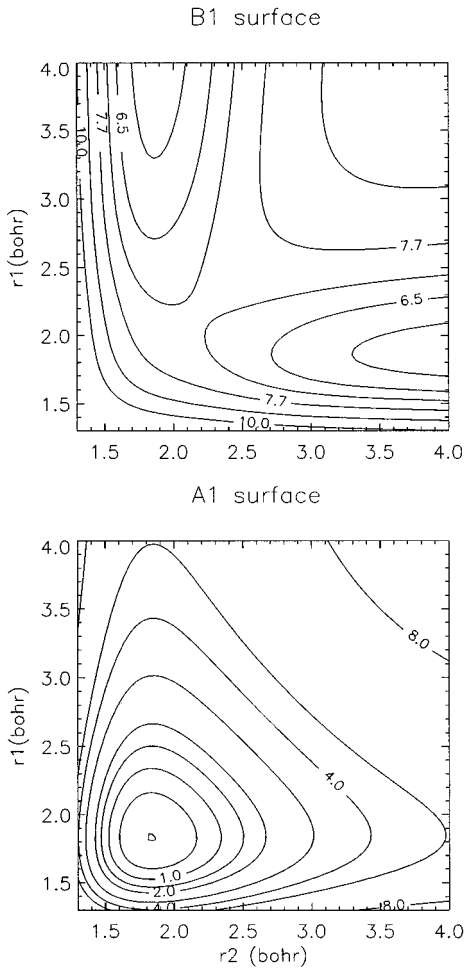

FIG. 1. Contour plots of the DFT potential energy surfaces for the A_1 ground state and the B_1 excited state are shown. The intermediate contours in the B_1 plot are for 6.0, 7.0, and 8.7 eV, and the intermediate contours in the A_1 plot are for 0.5, 1.5, 3.0, and 5.0 eV.

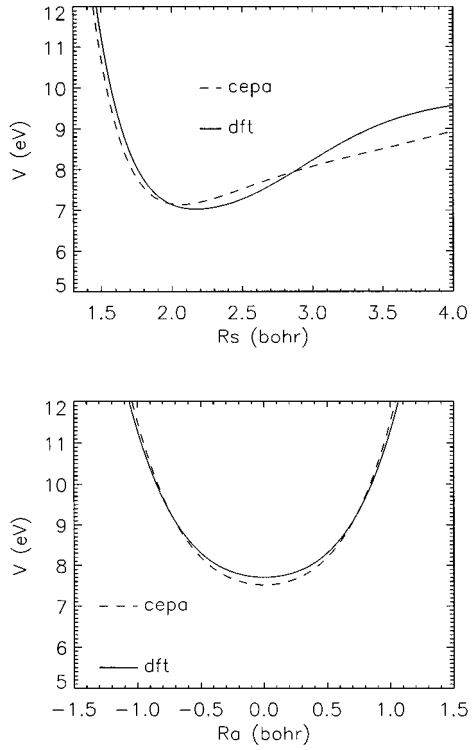

FIG. 2. The DFT B_1 potential energy surface is compared with the CEPA surface for (i) a cut along the symmetric stretch coordinate $R_s=(r_1+r_2)/2$, where $r_1=r_2$ (the upper plot) and (ii) a cut along the antisymmetric stretch coordinate $R_a=r_1-r_2$, for $R_s=1.8088\ a_0$ (the lower plot). The CEPA surface was positioned relative to the B_1 DFT surface by requiring that the vertical excitation energy relative to the A_1 DFT surface be 7.52 eV (Ref. 20) for $r_1=r_2=1.8088\ a_0$.

agreement with the experimental value for the electronic energy release (2.30 eV, see Table III). Actually, the agreement between DFT and ''experiment'' is somewhat worse for the electronic energy release than for the vertical excitation energy. The better agreement for the vertical excitation energy is due to a cancellation of errors; The dissociation energy we calculate by subtracting the asymptotic energy of OH+H from the ground state energy of water is 5.54 eV which is slightly too large compared to the experimental value (5.45 eV) obtained from D_0 (Ref. 45) and zero-point vibrational energies of water and OH.

We now turn the attention to the 2D potential energy surfaces calculated for the ground $\tilde{X}\ ^1A_1$ state and the excited $\tilde{A}\ ^1B_1$ state, keeping the bond angle fixed at its ground state equilibrium value. Contour plots of the electronic energy as function of the two OH bond distances are shown for both electronic states in Fig. 1. The DFT $^1B_1$ PES is in agreement with that of Staemmler and Palma[20] in that it shows a saddle point which can only be reached by both bonds elongating simultaneously (the saddle point is at a value of $r_1=r_2=2.16\ a_0$). On the basis of the excited state PES, one would expect the trajectories to start predominantly along the C_{2v} axis ($r_1=r_2$) until the minimum at the saddle point is reached, at which point dissociation in to one of the two equivalent exit channels can proceed by continued elongation of now only one O–H bond.

For a more detailed comparison, we present in Figs. 2 and 3 several plots of both the DFT and the CEPA $^1B_1$ state PES, for fixed values of either the symmetric stretch coordinate $r_s=(r_1+r_2)/2$ [showing the dependence on the antisymmetric stretch coordinate $r_a=(r_1-r_2)$] or for fixed values of the antisymmetric stretch coordinate (showing the dependence on the symmetric stretch coordinate). The dependence of the $^1B_1$ potential along the symmetric stretch coordinate r_s is shown in Fig. 2 for $r_a=0$ (upper plot). Note that the DFT and the CEPA PES are of comparable steepness in the Franck–Condon region, although the saddle point is located at different values of r_s (at 2.04 a_0 in the CEPA PES, and at 2.16 a_0 in the DFT PES). In performing the dynamics, we may therefore expect to see more fragment vibrational excitation in the OH fragment when using the DFT surface.

The dependence of the CEPA and DFT potentials on the antisymmetric stretch coordinate r_a is shown in Fig. 2 for the ''Franck–Condon'' value of r_s (1.8088 a_0, lower plot). Note that the motion in this coordinate is bound in the Franck–Condon region, and that the DFT and CEPA curves are very similar.

In Fig. 3, we show the potential dependence along r_a for the r_s coordinate fixed at the saddle point found respectively

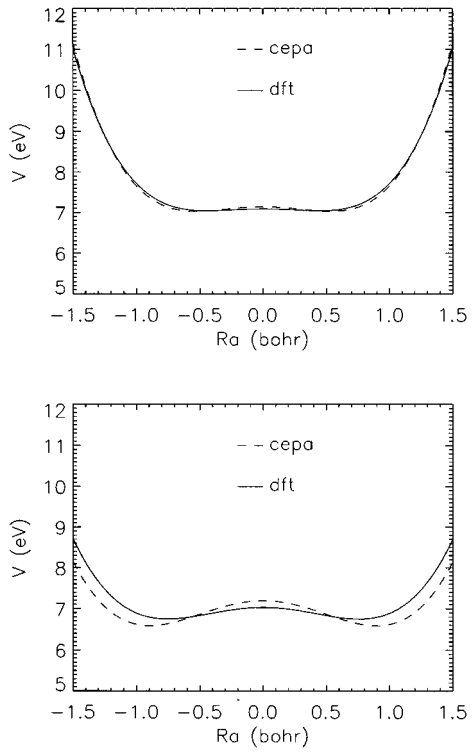

FIG. 3. The DFT B_1 potential energy surface is compared with the CEPA surface for (i) a cut along the antisymmetric stretch coordinate $R_a=r_1-r_2$ through the saddle point of the CEPA surface ($R_s=2.04\ a_0$, $R_a=0.0$, the upper plot), and (ii) a cut along the antisymmetric stretch coordinate R_a through the saddle point of the DFT surface ($R_s=2.16\ a_0$, $R_a=0.0$, the lower plot). The CEPA surface was positioned relative to the B_1 DFT surface as in Fig. 1.

in the CEPA calculations ($2.04\ a_0$, upper plot) and in the DFT calculations ($2.16\ a_0$, lower plot). For both values of r_s, the DFT curves show a smaller negative curvature $\partial^2 V/\partial r_a^2$. For geometries slightly away from the line $r_1=r_2$, the force pushing the system away from that line in to the dissociation channel will be proportional to $r_a\ \partial^2 V/\partial r_a^2$, which should mean that dissociation should proceed somewhat slower on the DFT potential energy surface, and that the molecule should be more likely to execute at least one vibration along the symmetric stretch coordinate before dissociating. This motion shows up as a recurrence in the autocorrelation function, which can lead to the presence of diffuse structure in the absorption spectrum.[23,24] We would thus expect that the smaller negative curvature of the DFT potential along r_a in the region close to the saddle point should lead to the presence of a more pronounced structure in the DFT spectrum.

Finally, we performed some checks to see whether DFT finds little anisotropy in the excited state potential close to the Franck–Condon region, as was found before in the CEPA calculations. Some results are shown in Table IV. As can be seen, the potential shows only a small dependence on the H–O–H angle over a large range of angles (from 80° to 140°, the maximum deviation is about 0.3 eV). We conclude that, as is the case for the CEPA surface, it should be a reasonable approximation to keep the H–O–H angle fixed at its ground state equilibrium value, only treating the two O–H stretches as degrees of freedom.

TABLE IV. Energy dependence of the first excited $\tilde{A}\ ^1B_1$ state along the bending coordinate $\alpha_{\mathrm{H-O-H}}$ in the Franck–Condon region described by $r_1=r_2=1.8088\ a_0$.

$\alpha_{\mathrm{H-O-H}}$ (deg)	$E(^1B_1)$ (eV)
80	−06.1389
100	−06.4869
120	−06.4251
140	−06.1875

B. Fits

The coefficients for the three-body potential resulting from fitting the DFT results to Eqs. (2.2)–(2.4) are given in Table V for both the A_1 ground state surface and the B_1 excited state surface. All other coefficients used in the fit expressions have already been given in Sec. II B. The largest deviation in the fit of the A_1 surface was 0.025 eV, and the largest deviation in the fit of the B_1 surface was 0.111 eV. However, the latter error in the fitting occurred at $(r_1,r_2)=(3.35a_0,\ 3.35a_0)$, and in the region enclosing the Franck–Condon point and the saddle point ($1.55\ a_0 \leqslant r_1,r_2 \leqslant 2.8\ a_0$) the largest error in the fit was only 0.031 eV.

C. Dynamics

As described in Sec. II B, the ground state vibrational wave function of the electronic ground state is required in the photodissociation calculations. This wave function and its energy were calculated variationally as described in Sec. II C. Using the A_1 potential fit to the DFT energies, the zero-point vibrational energy calculated for H_2O was 3655 cm^{-1}, in reasonable agreement with the zero-point vibrational energy calculated from the (experimental) Sorbie–Murrell potential[46,47] using the same (2D LHL) model (3859 cm^{-1}).

TABLE V. Fitting coefficients used in Eq. (2.4) are given for the DFT A_1 surface and for the DFT B_1 surface. In the coefficients, the distances are in Å and the energy is in eV.

i	P_i	$c_i(A_1)$	$c_i(B_1)$
1	1	−0.843 72	6.507 6
2	s_1+s_2	−1.428 1	7.159 1
3	$s_1^2+s_2^2$	−2.452 9	4.220 2
4	s_1s_2	−1.557 5	16.214
5	$s_1^3+s_2^3$	−2.691 0	−7.484 6
6	$s_1s_2^2+s_1^2s_2$	−4.453 5	18.915
7	$s_1^4+s_2^4$	10.786	13.851
8	$s_1s_2^3+s_1^3s_2$	−21.994	−25.037
9	$s_1^2s_2^2$	−16.612	54.556
10	$s_1^5+s_2^5$	−15.360	−5.261 3
11	$s_1s_2^4+s_1^4s_2$	19.588	5.966 2
12	$s_1^2s_2^3+s_1^3s_2^2$	−30.283	17.591
13	$s_1^6+s_2^6$	12.652	0.659 86
14	$s_1s_2^5+s_1^5s_2$	6.236 4	−2.672 7
15	$s_1^2s_2^4+s_1^4s_2^2$	67.503	0.609 77
16	$s_1^3s_2^3$	43.927	157.02

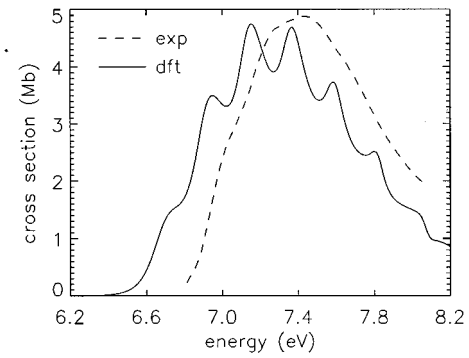

FIG. 4. The total cross section for photodissociation calculated using the DFT potential energy surfaces is compared with the experimental absorption spectrum (Fig. 1 of Ref. 48). Both are plotted as a function of the energy of the exciting radiation, and 1 Mb$=10^{-18}$ cm^2.

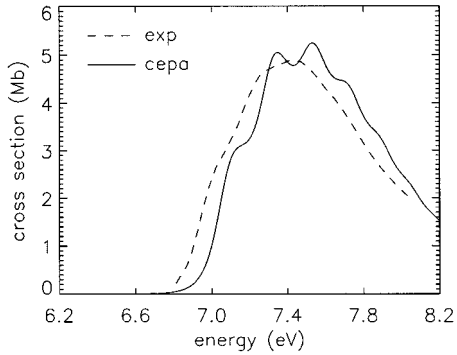

FIG. 5. The absorption spectrum calculated using the Sorbie–Murrel ground state surface (Refs. 46 and 47) and the fit of Engel *et al.* (Ref. 21) to the CEPA excited state surface (Ref. 20) is compared with the experimental absorption spectrum (Ref. 48). Both are plotted as a function of the energy of the exciting radiation, and 1 Mb$=10^{-18}$ cm^2.

The absorption spectrum calculated by putting the ground state vibrational wave function on the excited state surface and propagating it in time (see Sec. II C) is compared with the experimental gas phase photodissociation spectrum in Fig. 4. The experimental spectrum (Fig. 1 of Ref. 48) was obtained in the course of work on spectroscopy of H_2O in the gas phase and in the condensed phase. As can be seen, the agreement between theory and experiment is quite reasonable. If for the moment we exclude the enhanced structure in the DFT spectrum from consideration (see below), we find that the absorption bands have a similar shape and width. Better agreement would have been obtained in case the DFT spectrum would be shifted upwards by 0.1–0.15 eV, indicating that the vertical excitation energy we calculate (7.58 eV) is somewhat too low. This suggests that the actual vertical excitation energy should be in the range 7.68–7.73 eV. The fact that the overall shape of the DFT spectrum is correct and its position is in error by no more than 0.15 eV is certainly an encouraging result.

For comparison, we also show the spectrum obtained from a 2D LHL calculation using the fit of Engel *et al.*[21] to the excited state CEPA surface of Staemmler and Palma[20] in Fig. 5. In the calculations, we employed the Sorbie–Murrell ground state potential energy surface to generate the initial wave function, as was done by Engel *et al.*[21] As was done in the DFT calculations, a constant value was used for the transition dipole moment ($\mu=0.483$ atomic units, Ref. 21). As can be seen from comparing Fig. 5 with Fig. 4, the calculations using the CEPA surface result in better agreement with experiment. The SM-CEPA spectrum [the spectrum resulting from using the Sorbie–Murrell (SM) (Refs. 46 and 47) ground state surface and the CEPA excited state surface] would be in almost perfect agreement with experiment in case it were shifted downwards by 0.05–0.10 eV.

At first sight, it may seem strange that the SM-CEPA spectrum should lie at slightly higher energies than the experimental spectrum, which lies at higher energies than the DFT spectrum. As was mentioned in Sec. III A, the vertical excitation energy calculated using a CEPA treatment for both the ground state and the excited state surface (7.52 eV) (Ref. 20) is somewhat lower than the value calculated using DFT (7.58 eV). However, Engel *et al.*[21] did not fix the excited state CEPA surface and the ground state SM surface relative to one another by requiring that the CEPA surface be 7.52 eV higher than the SM surface at the ground state equilibrium geometry. Rather, the surfaces were fixed relative to one another by requiring that they go to the same asymptotic OH+H limit. One reason this procedure is likely to work well in a CEPA treatment is that the description of the unpaired $4a_1$ and $1b_1$ electrons in the excited state should put lower demands on the method used to describe their correlation than the description of the paired $1b_1$ electrons in the ground state. If the dissociation energy of the ground state is well known, in using an empirical ground state surface one may then avoid the possibility of the position of the absorption spectrum being affected by a possibly large error in the calculated ground state dissociation energy.

As a result of the method used to fix the SM and CEPA surfaces relative to one another, the vertical excitation energy effectively used in the dynamics calculations[21] is 7.79 eV rather than 7.52 eV. Thus, the good agreement of the SM-CEPA spectrum with experiment reflects the quality of the excited state CEPA potential energy surface, and the CEPA value for the electronic energy release should be quite good. The good agreement likewise reflects the correct imposition of the asymptotic OH+H limit on the Sorbie–Murrell empirical ground state surface. It is therefore not fully indicative of the quality of a full *ab initio* treatment (using *ab initio* surfaces for both electronic states). The fact that a lower value is obtained for the vertical excitation energy (7.52 eV) in a full CEPA treatment (both electronic states) than in a full DFT treatment (7.58 eV) indicates that the DFT spectrum we calculate should certainly be of comparable quality to the spectrum that would be obtained using a full *ab initio* treatment.

In a review paper, Engel *et al.*[19] note that the overall agreement between theory and experiment would slightly improve if the CEPA surface would be shifted downwards by 0.05–0.10 eV. This would then mean that the actual vertical excitation energy should be in the range 7.69–7.74 eV, in

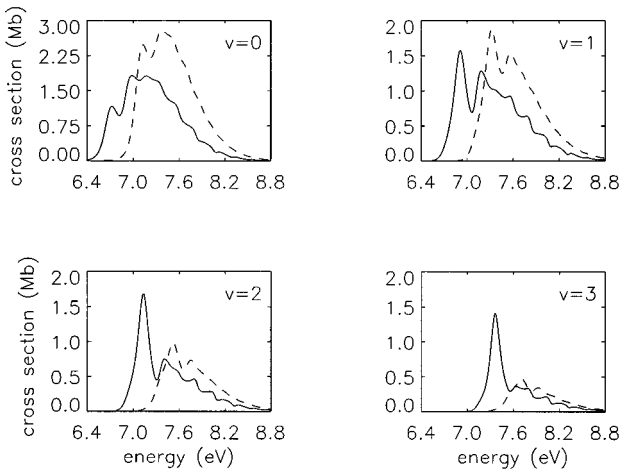

FIG. 6. Partial cross sections $\sigma_v(E)$ calculated using the DFT potential energy surfaces (full lines) are compared with the $\sigma_v(E)$ calculated using the Sorbie–Murrell ground state surface and the CEPA excited state surface (dashed lines) for $v=0$–3. The cross sections are plotted as a function of the energy of the exciting radiation, and 1 Mb$=10^{-18}$ cm^2.

agreement with what we found by comparing the DFT spectrum with the experimental spectrum.

Turning our attention back to Fig. 4, we find that a difference between the DFT spectrum and the experimental spectrum is that the DFT spectrum shows more structure. A comparison with Fig. 5 shows that the diffuse structure is also more pronounced in the DFT spectrum than in the SM-CEPA spectrum. However, from the comparison with experiment it is not entirely clear which calculation is better. It is known that much of the structure present in the 2D SM-CEPA spectrum disappears if the bending degree of freedom is also introduced, in a calculation for a single value of the total angular momentum quantum number J ($J=0$).[22] Likewise, the structure in a 3D ($J=0$) DFT spectrum should be less pronounced than that of the 2D DFT spectrum shown in Fig. 4. A further diminishing of the structure should result from averaging over the angular momenta J of H_2O (the experimental spectrum being taken at room temperature). The energy spacing between the diffuse bands is similar in the DFT spectrum (0.21 eV) of Fig. 4 and the SM-CEPA spectrum (0.2 eV) of Fig. 5. The structure in the spectra results from part of the wave packet carrying out one symmetric stretch vibration before dissociating.[23,24] The structure being more pronounced in the DFT spectrum should result from the coupling to the dissociative degree of freedom being weaker at the saddle point in the DFT surface (see Fig. 3), making it easier for the wave packet to carry out at least one symmetric stretch vibration.

Cross sections $\sigma_v(E)$ which are resolved with respect to the final vibrational state of the OH fragment are compared in Fig. 6, for the calculation using the DFT surfaces and the SM-CEPA calculation. There are clear differences between the vibrationally resolved DFT spectra and SM-CEPA spectra. Within the DFT treatment, the OH fragment resulting from dissociation is vibrationally hotter than within the SM-CEPA treatment; The average fragment vibrational energies are 6280 cm^{-1} (DFT) and 5131 cm^{-1} (SM-CEPA), respectively (these numbers include the OH zero-point vibrational energy, which is 1844 cm^{-1} using the present potential models). The fragment vibrational excitation can be attributed to the molecule's initial motion towards the saddle point, in which both bond lengths are stretched simultaneously prior to dissociation.[49] The hotter fragment vibrational distribution seen in the DFT calculation probably results from the saddle point being further away from the Franck–Condon region in the DFT excited state surface (the DFT saddle point lies at 2.16 a_0, whereas the CEPA saddle point is at 2.04 a_0, see also Fig. 3).

For a wavelength of 157 nm (7.9 eV), both the DFT and the SM-CEPA results are in good agreement with the experiments of Andresen *et al.*[14] In their experiment, the ratios $\sigma_0:\sigma_1:\sigma_2=1:1:0.58$, where the $v=2$ value has been corrected for the rapid predissociation taking place within the electronically excited state of OH.[21] From the DFT calculation, we find $\sigma_0:\sigma_1:\sigma_2=1:0.96:0.69$, and from the SM-CEPA calculation, we find $\sigma_0:\sigma_1:\sigma_2=1:0.80:0.49$. However, it should be pointed out that there is some controversy regarding the measurement of the OH vibrational state distribution: Mikulecky *et al.*[17] have measured a ratio $\sigma_0:\sigma_1=1:0.56$ for the same wavelength. Measurements have also been performed for a wavelength of 177.3 nm (6.99 eV).[18] However, at this excitation energy the partial $v=1$ cross section is just starting to become larger than zero in the SM-CEPA treatment, and the DFT results may well be in error due to the DFT vertical excitation energy being too low. The controversy regarding the fragment vibrational state population would be easier to resolve if experimental results were also available at a wavelength closer to the peak maximum (approximately 165 nm).

Because the fragment vibrational excitation is largely a result of the molecule's initial motion towards the saddle point, one might say that a comparison of theoretical and experimental partial vibrational cross sections should be indicative of the quality of the excited state potential energy surface along the symmetric stretch coordinate, in the area extending from the Franck–Condon point towards the saddle point. Based on the comparison with experiment at $\lambda=157$ nm alone, we cannot say, whether or not the quality of the DFT surface is comparable to that of the CEPA surface (the surfaces are different, see Fig. 2). The quality of the excited state surface in the same region can also be assessed by calculating a resonance raman emission spectrum and comparing with experiment. Because the emission spectrum is much more sensitive to the ground state potential energy surface,[25,26,50] to assess the quality of the DFT excited state potential energy surface it would be best to use an empirical ground state surface. Such calculations are outside the scope of the present work, where we investigate the validity of a full DFT approach to photodissociation. In closing, we should however mention that the good agreement obtained with emission experiments in calculations using the CEPA excited state surface[25–28] certainly indicates that the CEPA surface is of high quality in the region discussed.

IV. CONCLUSIONS

In order to test the validity of the DFT for calculating excited electronic states, we have performed DFT calculations on the first excited ($\tilde{A}\ ^1B_1$) state of H_2O. The photodissociation of H_2O through this state is a benchmark example of direct dissociation proceeding on a single electronic surface. Because the first excited singlet state $\tilde{A}\ ^1B_1$ is the lowest state of its symmetry also in the C_s symmetry applicable to dissociating geometries, a DFT treatment is formally justified. In practice one has to resort to approximations, such as the generalized gradient approximation for the exchange-correlation functional, and to the method for calculating multiplet splittings (singlet–triplet splitting in the present case) of Ref. 9. Our results therefore provide a test for the application of these approximations to the calculation of an excited state surface.

We have tested the results of the DFT calculations on the first excited ($\tilde{A}\ ^1B_1$) state by a direct comparison with previously performed, high level (CEPA) *ab initio* calculations. The vertical excitation energy obtained using DFT is in very good agreement with the CEPA result, but the electronic energy release is somewhat too low. There are some subtle differences between the CEPA and DFT potential energy surfaces, like the location of the saddle point (somewhat further away from the Franck–Condon region when using DFT), and the degree of coupling to the dissociative continuum close to the saddle point (the coupling being somewhat less in the DFT case).

Further tests of the DFT calculations were made by performing wave packet calculations on the photodissociation. Here, the bond angle was kept fixed at its ground state equilibrium value. The calculations were performed within a full DFT treatment, meaning that we also used a DFT surface for the electronic ground state. In this sense our calculations present a more severe test of the electronic structure method used than previous calculations, which used empirical surfaces for the electronic ground state.

The absorption spectrum calculated using the full DFT approach is in good agreement with the experimental spectrum, both in its overall shape and width and in the location of the absorption band. Still better agreement would have been obtained if the DFT spectrum would be shifted upward by 0.1–0.15 eV, indicating that the vertical excitation energy calculated using DFT is in error by no more than 0.15 eV. This is certainly an encouraging result. It is our hope that DFT will turn out to be useful also for investigating the photodissociation of other molecules. Given the success of our calculations, further research in this direction is certainly warranted.

On a level of increased detail, the DFT absorption spectrum shows too much structure compared to the experimental spectrum, but much of this should go away if a 3D treatment were used and with averaging over different initial rotational states of H_2O. Given that, it is not really clear whether the more pronounced structure we find in the 2D DFT spectrum indicates that the DFT potential energy surface is in error.

We have also calculated partial photodissociation cross sections which are resolved with respect to the final vibrational state of the OH fragment. For a wavelength of 157 nm, the DFT results are in good agreement with the results of dynamics calculations using the *ab initio* CEPA surface, and also with the experimental results of Andresen *et al.*[14] However, it should be noted that there exists a controversy regarding the measurement of the OH vibrational state distribution. Measurements of this distribution for excitation energies closer to the maximum in the absorption spectrum would be welcomed. Such measurements would constitute tests of the excited state potential energy surfaces in the region ranging from the Franck–Condon region to the region around the saddle point, in which there are some subtle differences between the DFT and the CEPA surface.

For the test case considered here, DFT in conjunction with the use of a GGA has shown itself to be both a useful and accurate tool for calculating a potential energy surface for an electronically excited state of a polyatomic molecule. While DFT is perhaps not as accurate yet as high level *ab initio* theory, it is certainly more readily applicable to large molecules, due to a more favorable scaling of the cost of a calculation with the number of electrons modeled. Consequently, DFT may be quite useful to model the photodissociation of large molecules possessing a high degree of symmetry, like $Mn_2(CO)_{10}$. In calculations on this molecule,[51] it was found that accurate vertical excitation energies can be obtained for a large number of states. Our present results suggest that it should also be possible to calculate reliable potential energy surfaces for such molecules, for geometries representing bond breaking situations in which all or part of the symmetry of the molecule is conserved.

ACKNOWLEDGMENTS

We thank R. Schinke for providing us with the fit of the excited state potential energy surface. We would also like to thank M. C. van Hemert for providing us with an experimental spectrum, and for helpful discussions. This research was made possible through financial support by the Royal Netherlands Academy of Arts and Sciences (KNAW) and by the E.E.C. ''Human Capital and Mobility'' program.

[1] *Density Functional Methods in Chemistry*, edited by J. K. Labonowsky and J. Andzelm (Springer, New York, 1991).
[2] T. Ziegler, Chem. Rev. **91**, 651 (1991).
[3] P. Hohenberg and W. Kohn, Phys. Rev. **136B**, 864 (1964).
[4] A. D. Becke, Chem. Phys. **84**, 4524 (1986); Phys. Rev. A **38**, 3098 (1988).
[5] J. P. Perdew, Phys. Rev. B **33**, 8822 (1986); **34**, 7046 (1986).
[6] M. Lannoo, G. Baraff, and M. Schlüter, Phys. Rev. B **24**, 943 (1981).
[7] E. U. K. Gross, L. N. Oliveira, and W. Kohn, Phys. Rev. A **37**, 2805 (1988); **37**, 2809 (1988); **37**, 2821 (1988).
[8] A. Nagy and Andrejkovics, J. Phys. B **27**, 233 (1994).
[9] T. Ziegler, A. Rauk, and E. J. Baerends, Theor. Chim. Acta **43**, 261 (1977).
[10] U. von Barth, Phys. Rev. A **20**, 1693 (1979).
[11] T. Ziegler, J. K. Nagle, J. G. Snijders, and E. J. Baerends, J. Am. Chem. Soc. **111**, 5631 (1989); A. Rosa and E. J. Baerends, Inorg. Chem. **33**, 584 (1994); C. Daul, E. J. Baerends, and P. Vernooijs, *ibid.* **33**, 3543 (1994).
[12] J. H. Wood, J. Phys. B **13**, 1 (1980).
[13] H.-t. Wang, W. S. Felps, and S. P. McGlynn, J. Chem. Phys. **67**, 2614 (1977).
[14] P. Andresen, G. S. Ondrey, B. Titze, and E. W. Rothe, J. Chem. Phys. **80**, 2548 (1984).
[15] D. Häusler, P. Andresen, and R. Schinke, J. Chem. Phys. **87**, 3949 (1987).
[16] R. L. Vander Wal, J. L. Scott, and F. F. Crim, J. Chem. Phys. **92**, 803 (1990).
[17] K. Mikulecky, K.-H. Gericke, and F. J. Comes, Chem. Phys. Lett. **182**, 290 (1991).

[18] K. Mikulecky, K.-H. Gericke, and F. J. Comes, Ber. Bunsenges. Phys. Chem. **95**, 927 (1991).
[19] V. Engel, V. Staemmler, R. L. Vander Wal, F. F. Crim, R. J. Sension, B. Hudson, P. Andresen, S. Hennig, K. Weide, and R. Schinke, J. Phys. Chem. **96**, 3201 (1992).
[20] V. Staemmler and A. Palma, Chem. Phys. **93**, 63 (1985).
[21] V. Engel, R. Schinke, and V. Staemmler, J. Chem. Phys. **88**, 129 (1988).
[22] M. von Dirke and R. Schinke, Chem. Phys. Lett. **196**, 51 (1992).
[23] M. Braunstein and R. T. Pack, J. Chem. Phys. **96**, 891 (1992).
[24] N. E. Henriksen, J. Zhang, and D. G. Imre, J. Chem. Phys. **89**, 5607 (1988).
[25] R. J. Sension, R. J. Brudzynski, B. S. Hudson, J. Zhang, and D. G. Imre, Chem. Phys. **141**, 393 (1990).
[26] J. Zhang and D. G. Imre, J. Chem. Phys. **90**, 1666 (1989).
[27] S. Hennig, V. Engel, R. Schinke, and V. Staemmler, Chem. Phys. Lett. **149**, 455 (1988).
[28] R. L. Vander Wal, J. L. Scott, F. F. Crim, K. Weide, and R. Schinke, J. Chem. Phys. **94**, 3548 (1991).
[29] G. J. Kroes, J. Chem. Phys. **101**, 5792 (1994).
[30] E. J. Baerends, D. E. Ellis, and P. Ros, Chem. Phys. **2**, 41 (1973).
[31] G. te Velde and E. J. Baerends, J. Comput. Phys. **99**, 84 (1992).
[32] S. H. Vosko, L. Wilk, and M. Nusair, Can. J. Phys. **58**, 1200 (1980).
[33] B. J. Rosenberg and I. Shavitt, J. Chem. Phys. **63**, 2162 (1975).
[34] E. J. Heller, J. Chem. Phys. **68**, 2066 (1978).
[35] G. G. Balint-Kurti, R. N. Dixon, and C. C. Marston, J. Chem. Soc. Faraday Trans. **86**, 1741 (1990).
[36] D. C. Clary and J. P. Henshaw, in *The Theory of Chemical Reaction Dynamics*, edited by D. C. Clary (Reidel, Dordrecht, 1986), pp. 331–358.
[37] G. G. Balint-Kurti, R. N. Dixon, and C. C. Marston, Int. Rev. Phys. Chem. **11**, 317 (1992).
[38] J. Tennyson and B. Sutcliffe, J. Chem. Phys. **77**, 4061 (1982).
[39] S. Carter and N. C. Handy, Mol. Phys. **47**, 1445 (1982).
[40] T. J. Park and J. C. Light, J. Chem. Phys. **85**, 5870 (1986).
[41] D. Kosloff and R. Kosloff, J. Comp. Phys. **52**, 35 (1983).
[42] G. J. Kroes, E. F. van Dishoeck, R. A. Beärda, and M. C. van Hemert, J. Chem. Phys. **99**, 228 (1993).
[43] R. Meyer, J. Chem. Phys. **52**, 2053 (1970).
[44] C. C. Marston and G. G. Balint-Kurti, J. Chem. Phys. **91**, 3571 (1989).
[45] G. Herzberg, in *Electronic Spectra and Electronic Structure of Polyatomic Molecules* (Krieger, New York, 1991), Vol. III.
[46] K. S. Sorbie and J. N. Murrell, Mol. Phys. **29**, 1387 (1975).
[47] K. S. Sorbie and J. N. Murrell, Mol. Phys. **31**, 905 (1976).
[48] M. C. van Hemert and A. van der Avoird, J. Chem. Phys. **71**, 5310 (1979).
[49] R. Schinke, *Photodissociation Dynamics* (Cambridge University, Cambridge, 1993).
[50] G. J. Kroes and M. C. van Hemert, J. Chem. Phys. **100**, 1128 (1994).
[51] A. Rosa, G. Ricciardi, E. J. Baerends, and D. J. Stufkens, Inorg. Chem. (accepted).